DOCTORAL THESIS

Impact of statistical reconstruction and compressed sensing algorithms on projection data elimination during medical X-ray computed tomography image reconstruction

（Ｘ線ＣＴ画像再構成における投影データの削減に対する統計的再構成法および圧縮センシングアルゴリズムの影響）

KITAMI INSTITUTE OF TECHNOLOGY

DOCTORAL COURSE OF MEDICAL ENGINEERING

SUN BINGYU

（孫 氷玉）

March 2018

Contents

Chapter 1. CT reconstruction technology

1.1. Principle of CT Reconstruction

Dr. J. Radon proved that "Any object can be reconstructed to two-dimensional or three-dimensional image with projection data of its own." This is the mathematical basis of the reconstruction of CT projection image.[1]

Collection of projection data of CT is shown in Fig. 1, where r stands for position of parallel movement, θ stands for angle of rotation. X ray source and X detector are placed on the two sides of scanned object. The X-ray tube rotates by scanned object, and horizontal movement is also made in perpendicular to the rotation axis. X ray is attenuated during passing through scanned object, and detectors, after collecting data collection set ρ(θ，r), sends these data to computers for image reconstruction to get CT images of scanned object.

ρ（θ，r）is taken as the projection of f(x,y), and is called "sinogram" as shown in figure 2. During the process, the transformation of f(x,y) to ρ（θ，r）is called "Radom transformation". The calculation process of getting the value of f(x,y) by solving out the solution to ρ(θ，r) is called "Image Reconstruction" (Fig. 2).

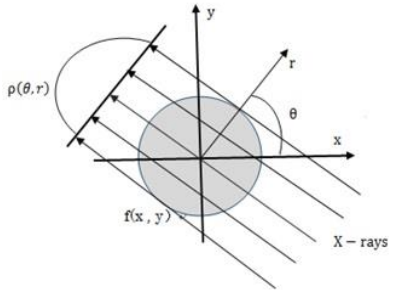

Fig.1 Principle of CT Reconstruction

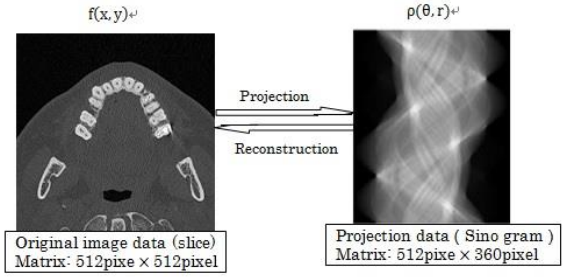

Fig.2 Projection and reconstruction schematic

1.2 Back projection reconstruction

The simplest method for image composition is the back projection calculation of projection data, which is called "Back-Projection" (Fig. 3). "Back-Projection" is a process where each pixel point passing through X ray is assigned, along the projection direction, the same projection value using acquired projection data. Image acquired by summation of back projection value along a projection direction is termed as a back projection image. The whole back projection process is shown in Fig. 3. The back projection's verification is conducted by choosing a known 2*2 matrix and projection samples got by angles 0, 45, 90 and 135. At first, projection data along the corresponding direction is got by the summation of two elements in the horizontal direction of a prior image, and then the back projection is conducted towards a new matrix along the same projection direction using acquired data until the projection is

ended.

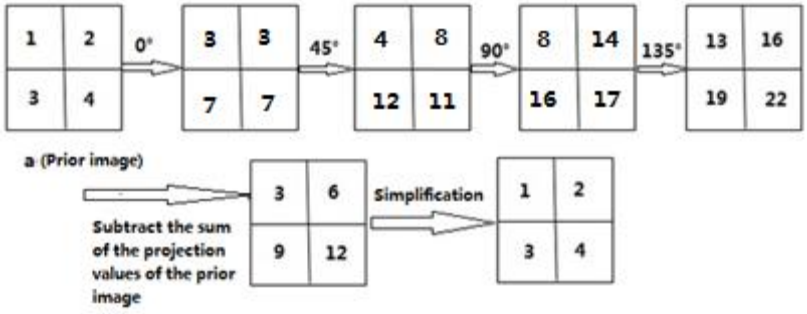

Fig.3 Inverse projection iteration process

As shown in Fig. 3, the projection value $g(x,y)$ gotten after iteration by the angle of 135 degree is inconsistent with $f(x,y)$ of the prior image with significant difference. The prior image $f(x,y)$ and reverse projection matrix $g(x,y)$ can be represented using a point spread function.

Chapter 2. CT reconstruction algorithm

2.1 Image acquisition

With the approval of IRB, two CT images of the maxilla in a single series were used for the study (Fig. 4: A and B). A spiral CT scanner, Somatom(TM) Plus 4 Volume Zoom (Siemens, Erlangen, Germany) was utilized. Exposure conditions were as follows: 120kV, 130 mAs, 0.5mm slice thickness. The size of a CT image is 512 x 512. The image data sets were processed by means of the manipulation of the projection data to simulate difference in data quantity and distribution.

Projection data acquisition was carried out as described in previous reports [2-5]. Each pixel of the image has a CT number, which is proportional to X-ray's transparency. The shape of each pixel is a trapezoid, depending on the angle between the projection and each pixel square. During the detectability calculation, the pixel value is accumulated by adding the respective pixels' CT numbers. If the shape of the projection is not square, the detectability will be divided by the center of the detector element and neighboring elements. The image matrix contained 512 pixels. The projection data were acquired in 360 directions at 1° intervals, so the pixel number was 512 x 360. Details were described in previous report, Dong *et al*. 2014.[5]

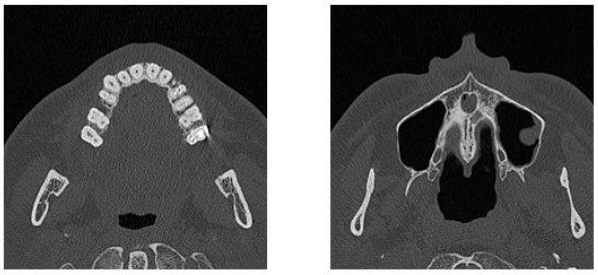

A B

Fig.4 Two original images:Left(image A),a slice on maxilla level,Right(image B),a slice on maxillary

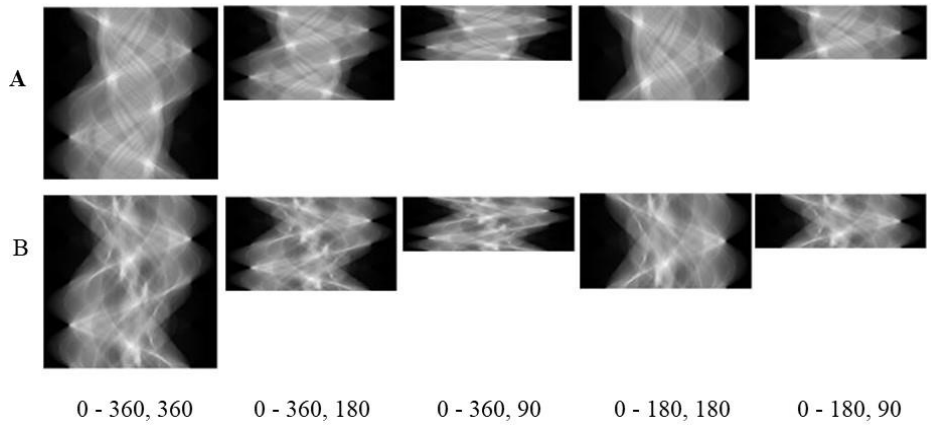

Fig. 5: Projection data (sinogram) of image A (top row) and image B (bottom row). Sampling range and the number of projections are, 0°-360° & 360, 0°-360° & 180, 0°-360° & 90, 0°-180° & 180, and 0°-180° & 90, respectively, from left to right.

The projection data to be used for the CT image reconstruction was adjusted by selective removal of data. First, data intervals were increased from 1° to 2° or 4°, the number of projection data being reduced from 360 to 180 and 90, respectively. Second, sampling range of projection data was reduced from 0° - 360° to 0° - 180°. Third, limited sampling range was combined with increased data intervals. Fourth, further projection data elimination was tried by using the total variation minimization method applying compressed sensing. For this, both 45 and 36 were set for the number of projection data in the range of 0° to 180° (4° and 5° intervals respectively). Settings utilized are summarized in Table 1 and individual projection data are shown as sinograms are illustrated in Fig. 5.

Table 1 Projection data setting for elimination: Combinations of sampling range, the number of projection and intervals

Sampling range (degree)	The number of projection	Intervals (degree)
0 – 360	360	1
0 – 360	180	2
0 – 360	90	4
0 – 180	180	1
0 – 180	90	2
0 – 180	45	4
0 – 180	36	5

2.2 Algebraic reconstruction

ART is an algebraic image reconstruction method[6-8], converting the problem of image reconstruction into a linear equation (2). The formula is the equation between image and projection; $f = (f_1, f_2 \ldots f_m)^T$, a set of pixel values (vector space); $p = (p_1, p_2 \ldots . p_n)^T$, a set of observed projection data (vector space); $W=\{w_{mn}\}$, M x N dimension matrix of coefficients; w_{mn}, crossing length on a pixel(n-th) and X-ray projection (m-th).

The formulation of the ART algorithm is described as follows:

$$f_j^{(k+1)} = f_j^{(k)} + \frac{P_i - \sum_{n=1}^{N} w_{in} f_n^{(k)}}{\sum_{n=1}^{N} W_{in}^2} w_{ij} \qquad (1)$$

Chapter 3. Reconstruction algorithm based on compressed sensing

3.1 Sparse representation of image

The compressed sensing [9] theory proposed by D. Donoho et al. [10] in 2006 provided a theoretical and technical basis for CT image reconstruction in the condition of incomplete data acquisition. The theory suggested that the original signal could be restored by an appropriate optimization if the signal is sparse (or can be indicated sparsely) and the data is sampled at a lower rate than the Nyquist frequency derived from Shannon's theorem.

Based on the compressed sensing theory, CT images have sparse properties; however, medical images are actually not sparse. Under general circumstances, pixel can have a value other than zero. By means of a transformation, it is possible to enable that most image pixels to tend to zero. As a result, assuming that pixel values in the same texture in CT images are the same and changes in pixel values only occur at edges of the texture, the image can be

transformed by using the gradient magnitude of the CT image to become approximately sparse (Fig. 6). This process is "Discrete Gradient Transformation".[11-14]

$$\left\|\vec{f}\right\|_{\mathrm{TV}} = \sum_{m=1}^{M}\sum_{n=1}^{N}((f_{m+1,n} - f_{m,n})^2 + (f_{m,n+1} - f_{m,n})^2)^{\frac{1}{2}} \approx \left\|\nabla\overrightarrow{f_{mn}}\right\|_{l1} \quad (2)$$

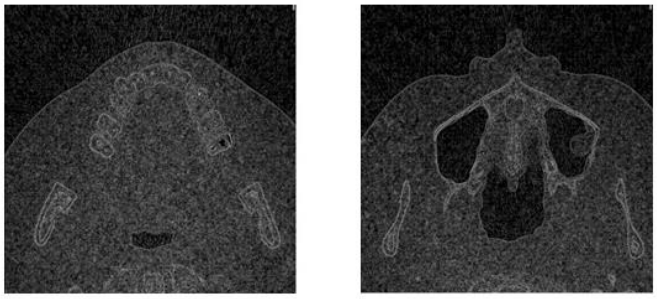

A B

Fig.6: Two images, corresponding to original images in Fig.4,transformed by using the gradient magnitude.

The matrix, (m ,n) represents the coordinate on image in horizontal and vertical directions, and $f_{m,\,n}$ represents the gray value of pixel, which indicates the degree of change in concentration according to equation (2).

3.2 CT image reconstruction algorithm based on total variation (ART-TV)

In 2006, Sidky et al. [14-15] proposed a so-called ART-TV method, which is based on the minimization of TV, and transformed the CT reconstruction problem into a constrained optimization problem. Its reconstructed image model is expressed as

$$minTV(f) \quad s.t. \;\; Wf = P \qquad . \qquad (3)$$

In Eq. (6), W denotes the projection coefficient matrix, P the projection value, and f the image pixel. The total variance definition of image f is

$$TV(f) = |\nabla f| = \sum_{i,j}\sqrt{(\nabla_x f)^2 + \left(\nabla_y f\right)^2 + \varepsilon}. \qquad (4)$$

where $f_{i,j}$refers to the gray value of the image F at the pixel point (i, j), and ε is a small positive constant that avoids discontinuities. The gradient descent method is generally adopted to solve the minimum TV value, and its iterative equation is expressed as

$$f_{i,j}^{(k+1)} = f_{i,j}^{(k)} - \alpha\frac{\partial TV\left(f_{i,j}^{(k)}\right)}{\partial f_{i,j}^{(k)}} \qquad (5)$$

3.3 Prior-image-constrained compressed sensing

In 2008, Chen et al. [16-17] proposed a reconstruction method of prior-image-constrained

compressed sensing for low-dose CT reconstruction. The high-quality CT image obtained from the patient pre-scans is used as a prior image (PI) of the current scan, and the average pixel values of homogeneous material in the prior image are extracted to form a prior value set, which will be introduced into the reconstructed image objective function to constrain the image to be reconstructed, so that the quality of the reconstructed image can be greatly improved. The mathematical model of the PICCS algorithm is expressed as

$$\min \ \alpha TV(f) + (1-\alpha)TV(f - f^{pr}) \qquad s.t \qquad Wf = P \qquad (6)$$

where f^{pr} refers to the prior image, and α refers to weight factor, with a value in the range from 0 to 1. If $\alpha = 1$, the algorithm is equivalent to the traditional TV algorithm.

The procedure for the PICCS algorithm is as follows:

(1) Initialize the reconstruction image f = 0, and relevant parameters;

(2) Using initial value u and projection data, use ART technique reconstruction once, and obtain an upgraded u;

(3) Obtain f* after minimization solution for equation (1) using a GDT;

(4) Go back to step (2), repeat f* as an ART reconstructed initial image, and execute step (2) and repeatedly until convergence is met.

Chapter 4. The influence of successive approximation and compressive sensing on the reduction of projection data of X-ray CT image reconstruction

4.1 Summary

CT (computed tomography) imaging technology has achieved shorter scanning times for each section and enabled simultaneous acquisition of multiple sections. Three-dimensional image processing and visualization techniques have been developed to support clinical demands. Greater use of CT technology, however, has resulted in delivering increased absorbed doses to patients. Statistical reconstruction methods used for CT image reconstruction have been applied clinically. Over the past decade, this development has brought new standards for reducing radiation exposure while achieving clinically acceptable image quality.

Computed tomography scanning (computed tomography, CT) plays a more and more important role in people's life. Now the algorithms used in CT reconstruction includes two types: analytic algorithm and iterative algorithm. The representative algorithm of analytic algorithm is filtered back projection (FBP) reconstruction method, its principal is: firstly, the

projection data is filtered, then projected back to the original image by the original path, and the projection data of all angles are superimposed to obtain the required fault image. The advantage of this algorithm is that it is simple, the reconstruction speed is fast, and the edge of the image will appear vague or star shaped artifacts. The iterative algorithm includes algebraic iterative method and statistical iterative method. Algebraic iteration is an algorithm based on the theory of solving equations, and the representative algorithm is Algebraic Reconstruction Technique (ART). But it has large amount of calculation with long construction time. The statistical iteration method takes the statistical properties of projection data into account, and represents Maximum Likelihood Expectation Maximization (ML-EM), etc. Under the assumption that projection data obeys Poisson distribution, the ML-EM algorithm establishes the imaging model, and its advantage is that the reconstructed image quality is better than the FBP algorithm, and the disadvantage is that the convergence speed is slow.

The sparse modeling theory permits fewer acquisition data to be used for complete reconstruction of signal, image, and audio processing. Compressed sensing is a solution for ill-posed inverse problems in image reconstruction, such as the sparse-view/under-sampling problem and noise removal from projection data. Total variation (TV) regularization is a key technology in determining the uniqueness of the solution.

The purposes of this study were to (1) examine the effect of statistical reconstruction algorithms and compressed sensing during TV regularization; (2) retain image quality despite projection data elimination; (3) explore the number and distribution of projection data needed to maintain adequate image quality; and (4) apply weighted TV values with prior image constraints.

Two CT images of the maxilla in a single series were used. Projection data acquisition was carried out. The projection data to be used for CT image reconstruction were adjusted by selective data removal. First, data intervals were increased from 1° to 2° or 4° and the number of projection data reduced from 360 to 180 and 90, respectively. Second, the sampling range was reduced from 0°–360° to 0°–180°. Third, the limited sampling range was combined with increased data intervals. Fourth, further projection data elimination was attempted using the TV regularization. For this step, the number of projection data were set at 45 and 36 in 0°–180° (at 4° and 5° intervals, respectively).

CT images were reconstructed following elimination of the projection data using the four methods. Whether the original image quality was maintained was evaluated in previous studies [Dong, J, et al. 2014, etc.]. It had been assumed that the use of 360 projection data collected in the range of 0°–360° at 1° intervals was sufficient to reproduce the original

quality. We aimed to investigate the possibility of further projection data manipulation in combination with statistical reconstruction algorithms. An algebraic reconstruction technique (ART) and the maximum likelihood-expectation maximization (ML-EM), an iterative restoration technique, were examined and compared with the traditional filtered back-projection (FPB), a standard inverse-Fourier transfer.

The compressed sensing theory proposed by Donoho, DL (2006) provided a theoretical and technical basis for CT image reconstruction under the condition of incomplete data acquisition. The theory suggested that, if the signal is sparse and the data are sampled at a lower rate than the Nyquist frequency, the original signal could be restored by appropriate optimization. Sidky, EY, et al. (2006) proposed the ART-TV technique based on TV regularization, which transforms the CT reconstruction issue to a constraint optimization problem.

When the sampling range was 0°–360°, image degradation by radial streak lines was apparent in the case of 4° intervals and 90 projections. But it is to a lesser extent on ART- and ML-EM-reconstructed images. When the range was 0°–180°, image degradation by radial streak lines was apparent, but the degradation was not as severe as the above case. The degradation on ART- and ML-EM-reconstructed images was less marked. When the ART-TV was applied for the combinations of 4° with 45 and 5° with 36 in 0°–180°, the image degradation was minimal despite the reduced projection data. When weighted TV values with prior image constraints were applied, images were reconstructed using sparse projection data without degradation.

The root-mean-square error and signal-to-noise ratio values both decreased with the reduced projection data, but the quality of the reconstructed images was best when using the ART-TV. Both ART and ML-EM required heavier calculation loading than FPB. Those for ART and ART-TV were compatible.

In conclusion, incomplete projection data due to either limited angle collection (from 360° to 180°) or thinning of the projection data (from 1° to 5° intervals) permit radiation dose reduction while sustaining image quality. It is achievable with the combination of statistical reconstruction algorithms and the compressed sensing method with TV regularization and prior image constraints. Despite heavier computational calculation loading, these methods should gain greater acceptance as computer calculation power continues to expand.

4.2 Materials and image

Original MDCT images processed in this study are the same as those used in previous

articles[2-3]. With Institutional Review Board approval, a CT image of the human maxilla was used for the study. The parameters of the X-ray CT machine and exposure conditions were as follows: machine, Somatom™ Plus 4 Volume Zoom (Siemens, Erlangen, Germany), 120kV; 130 effective mAs; 0.5mm in slice thickness; 512×512 pixel matrix. The original image datasets were processed by means of the manipulation of the projection data for purposes of this study.

The processing was executed using MATLAB software (Matlab R2015a version, MathWorks Japan, Tokyo) and C-language. The computer used was as follows: Intel Core i7-3770k CPU running at 3.50GHz, RAM: 32.0GB, Windows 7 (Microsoft Corporation, Redmond, WA, USA).

4.3. Image noise

In addition to a subjective and qualitative analysis of the image quality, Root-mean-square error (RMSE) and signal noise ratio (SNR) values were replenished to carry out quantitative and objective measurements of image noise.

The equations for calculating root-mean-square error and signal to noise ratio are as follows respectively:

$$RMSE = \frac{1}{M \times N} \sum_{\substack{0 \le n \le M \\ 0 \le m < N}} (f_{n,m} - f*_{n,m})^2$$

$$SNR = 10log\left(\frac{\sum(\bar{f}_{n,m} - f^*_{n.m})^2}{\sum(f_{n.m} - f^*_{n.m})^2}\right)$$

Where, M,N is the length and width of the image, $f_{m,n}$ indicates the pixel value of original image, $\bar{f}_{n,m}$ indicates the average of pixel values of original image, $f^*_{m,n}$ indicates the image pixel value to evaluated.

RMSE is used to judge the degree of distortion of reconstructed image from original image. The smaller RMSE value indicates that reconstructed image is closer to original image. SNR reflects the difference of noise level between original and reconstructed images in dB unit. A larger SNR value indicates better quality for the reconstructed image.

4.4 Comparison of algorithm based on sparse projection reconstruction

Reconstructed CT images using ART and ML-EM algorithms are shown (Figs. 7-9). The number of iteration were set at 100, 150 and 200, and restricted due to calculation loading. Only images after 100 times iterative processing are shown in this section.

Images shown in Fig. 7 are reconstructed CT images using projection data collected in the range of 0° to 360°. Sampling intervals and the number of projections are 2°, 180 and 4°, 90. In the case of 4° intervals and 90 projections, image degradation by radial streak lines was

apparent. This is clearly observed on FBP-reconstructed images and to a lesser extent on ART- and ML-EM-reconstructed images.

Images shown in Fig.8 are reconstructed CT images using projection data collected in the range of 0° to 180°. Sampling intervals and the number of projections are 1°, 180 and 2°, 90. Image degradation by radial streak lines was apparent in both cases, but are not as severe compared with the case of 4° intervals and 90 projections in Fig. 4. Their appearances on ART- and ML-EM-reconstructed images were less marked in comparison with those seen on FBP-reconstructed images.

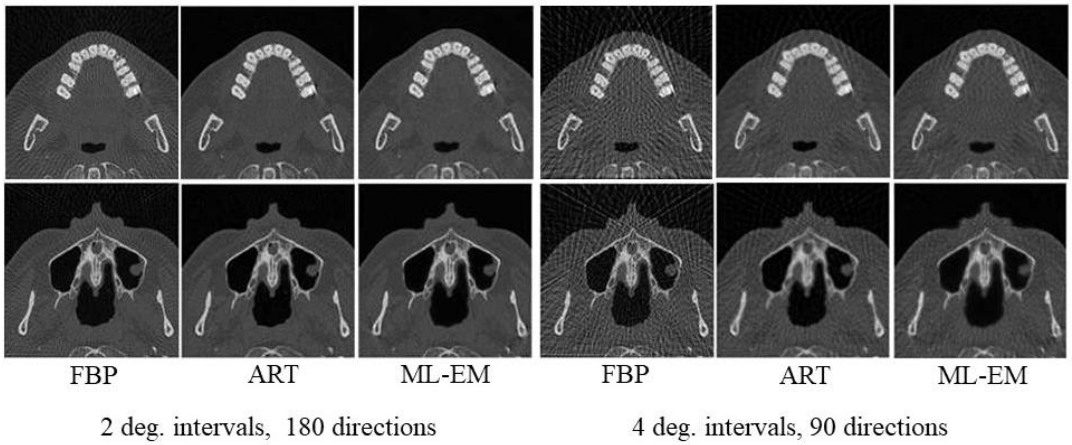

Fig. 7: Reconstructed CT images using projection data collected in the range of 0° to 360°. Sampling intervals and the number of projections are 2°&180 and 4°&90. Three kinds of

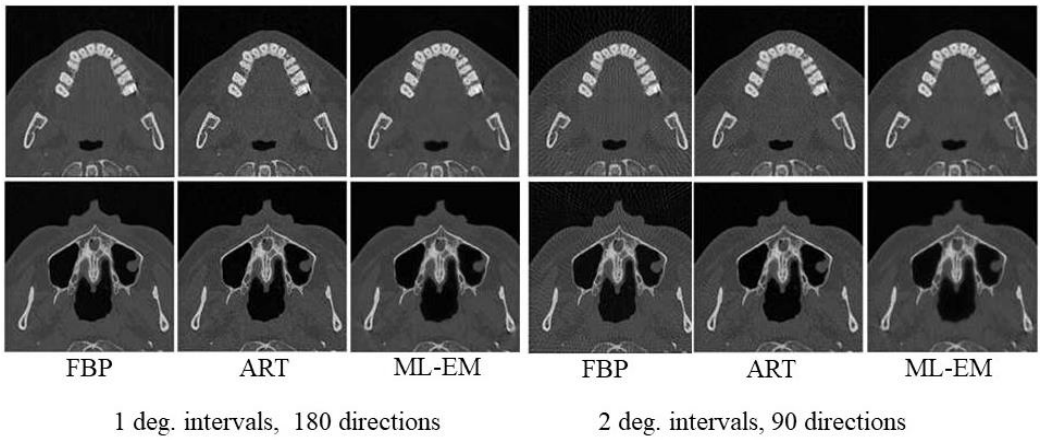

Fig. 8: Reconstructed CT images using projection data collected in the range of 0° to 180°. Sampling intervals and the number of projections are 1°&180 and 2°&90. Three kinds of reconstruction methods, FBP. ART and ML-EM were applied.

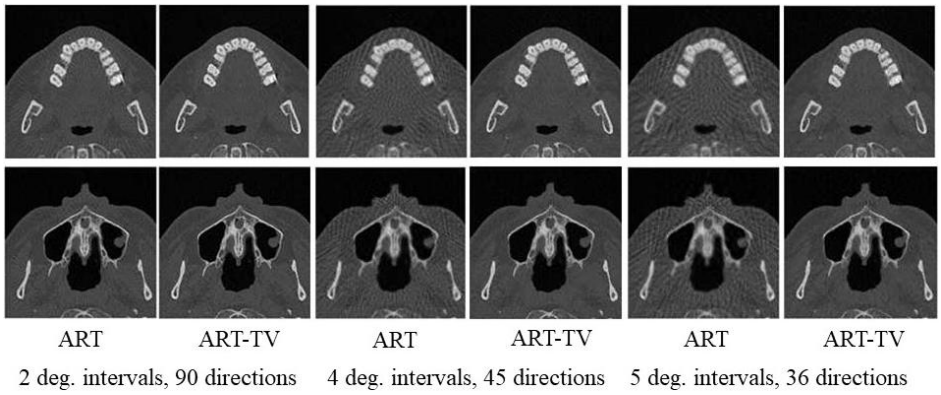

Fig. 9: Reconstructed CT images using projection data collected in the range of 0° to 180°. Sampling intervals and the number of projections are 2°&90, 4°&45 and 5°& 36. Two kinds of reconstruction methods, ART only and ART combined with total variation regularization

Images shown in Fig. 9 are reconstructed CT images using projection data collected in the range of 0° to 180°. Sampling intervals and the number of projections are 4°, 45 and 5°, 36. Only the ART combined with TV regularization (ART-TV) was applied. Compared with ART-reconstructed images, the image degradation by some radial streak lines became minimum in spite of the reduced number of projection data and ART-TV reconstructed images kept the image quality despite the highly reduced projection data utilized.

Results of subjective noise measurement are indicated in Figs.10 and 11. In Fig. 10, values of RMSE and SNR for different reconstruction methods, such as FBP, ART and ML-EM, result

in the images shown in Figs. 4 and 5. In Fig. 1, values of RMSE and SNR in the ART with and without TV regularization result in the images in Fig. 4. Both RMSE and SNR values decreased with the reduction of projection data, but the image quality constructed by ART-TV was the best. Image noise in reconstructed images varied with sampling range when the same number of projection data were obtained at different sampling intervals. The bigger the interval the worse the quality was. The quality of reconstructed image is the best by using ART algorithm with TV regularization in the study.

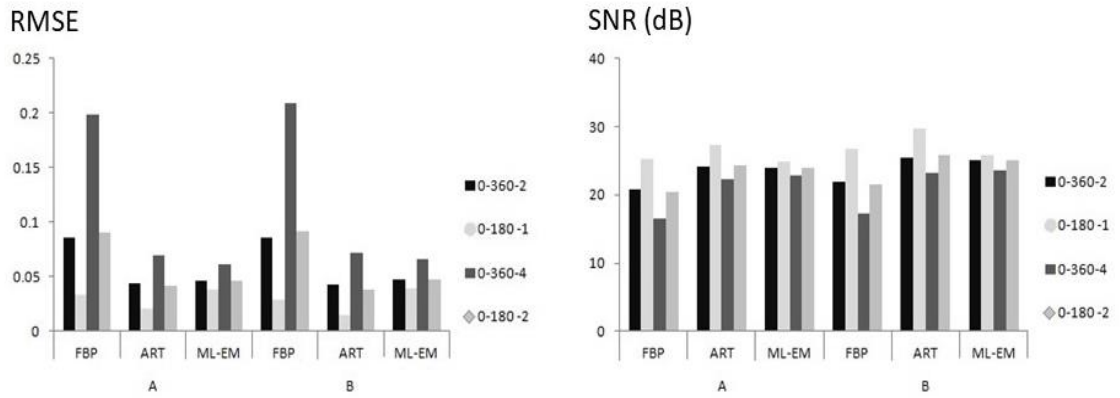

Fig. 10: RMSE and SNR values in images, which are corresponding to those in Fig. 8, reconstructed by three kinds of methods, FBP, ART and ML-EM. For example, "0-360-2" means that the projection data was collected in the range of 0° to 360° and the sampling interval is 2°. Symbols: A: image A, B: image B, which are same with those in Fig. 4.

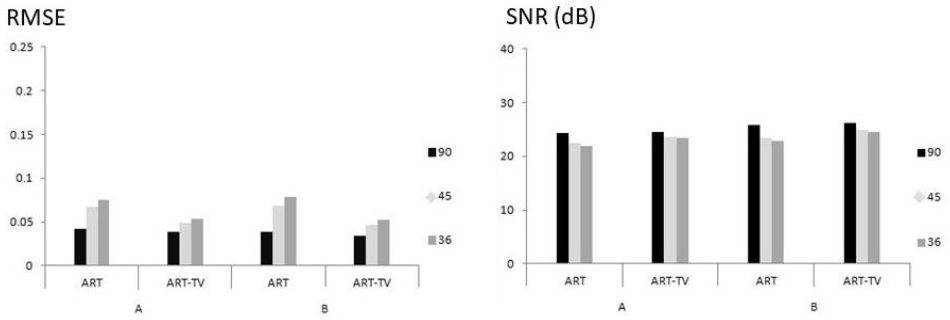

Fig. 11: RMSE and SNR values in images, which are corresponding to those in Fig. 9, reconstructed by two kinds of methods, ART only and ART combined with total variation regularization (ART-TV). The range of projection data collection was fixed at 0° to 180° . The number of projections were set at 90, 45 and 36. These are keys in the figure. Simultaneously these means that sampling intervals were set at 2°, 4° and 5°. Symbols: A: image A, B: image B, which are same with those in Fig. 4.

Table 2 Calculation loading: Duration times for processing every single CT slice, corresponding to images in Figures 9 and 10.

Sampling range (deg.)	The number of projection	FBP	ART	ML-EM
0 – 360	360	37 s	803min (13hr 23min)	25min
0 – 360	180	37 s	249min (4hr 9min)	17min
0 – 360	90	36 s	173min (2hr 53min)	10min
0 – 180	180	10 s	251min (4hr 11min)	15min
0 – 180	90	9 s	175min (2hr 55min)	11min

Table 3 Calculation loading: Duration times for processing every single CT slice, corresponding to images in Figure 11.

Sampling range (deg.)	The number of projection	ART		ART-TV	
		Image A	Image B	Image A	Image B
0 – 180	90	154min (2hr 34min)	153min (2hr 33min)	169min (2hr 49min)	162min (2hr 42min)
0 – 180	45	80min (1hr 20min)	79min (1hr 19min)	88min (1hr 28min)	88min (1hr 28min)
0 – 180	36	63min (1hr 3min)	65min (1hr 5min)	73min (1hr 13min)	72min (1hr 12min)

Note: Observed time, 154min (2hr 34min) at ART, 0-180 and 90, is slight different from 175min (2hr 55min) in Table 3, due to the performance difference of the PC used.

Tables 2 and 3 present calculation loadings (calculation times (s, min or hr/min) for processing a single CT slice). In comparison with FPB, both ART and ML-EM needed heavy calculation loadings (Table 2). Those of ART and ART-TV were compatible (Table 3).

4.5 Discussion

Image reconstruction from sparse view or noisy projection data has been studied previously for oral and maxillofacial radiology [20, 21]. Decreasing the number of projection views is regarded as an effective method for patients' dose reduction. The present study applied statistical reconstruction algorithms and compressed sensing methods in an attempt to provide a new solution to the problem.

Compared with the traditional FBP method, statistical reconstruction algorithms, ART and ML-EM, make possible the use of markedly reduced projection data, which in turn could results in dose savings. Fig. 4 and 5 show that the great difference found between FBP and statistical methods. In addition, the combination of intervals of the sampling changed from 1° to 4° and ranges of projection data (0° to 360° or 0° to 180°) affected outcomes. The reconstruction at 90 projections from 0° - 180° (Fig. 5) showed the much better objective image quality than that at 90 projections from 0° - 360° (Fig. 4). Figure 6 shows that the ART-TV regularization implemented method showed good image quality compared to ART alone.

To reduce the projection data, the thinning-out method with equal intervals was used. However, it is possible that equal interval need not always be used. This would provide for the possibility in future to choose the projection data distribution which is optimized for an

individual CT examination. For example it is thought that the thinning-out method with unequal intervals would be taken for avoiding metal-induced artifacts.

Image degradations that appeared on some images (Fig. 4 -6) were radial streak lines. Reducing these radial lines makes it possible to reduce the projection data further. Additional methods, such as nonlinear filtering, nonlinear sparsifying transform and edge-preserving method were recently proposed by researchers [22-25]. These methods give the possibility to reduce the projection data for CT image reconstruction in oral and maxillofacial imaging.

The drawback of statistical reconstruction is high and heavy calculation loadings as shown in Tables 2 and 3. If the ML-EM is replaced with the OS-EM (Ordered Subset-Expectation Maximization), the calculation loading is dramatically reduced. GPGPU (general purpose graphic processing unit) machine is also becoming less costly. These were proven in a limited way by our previous researches [4, 5].

In conclusion, incomplete projection data due to either limited angle collection (from 360° to 180°) or thinning of the projection data (from 1° to 5° intervals) can permit radiation dose reduction while sustaining image quality. This is achievable with the combination of statistical reconstruction algorithms, ART and ML-EM and the compressed sensing method with TV regularization. In spite of heavier computational calculation loadings, these methods should gain greater acceptance as computer calculation power continues to expand.

Chapter 5. CT Reconstruction algorithm based on weighted total variation

5.1 Summary

TV_POCS（total variation projections Onto Convex sets）algorithm (in 2006, it was raised by Sidky and X. Pan [14-15]) and Prior Image Constrained Sensing, PICCS reconstruction method (in 2008, it was raised by Chen [16-17]). Under the condition of sparse projection, the quality of the reconstructed image is very good. All the above algorithms use Total Variation (TV) transform as the sparse transform of the images. That is, using operators in two directions of horizontal and vertical to sparsely represent images. The TV algorithm has the possibility of improvement, as it does not make full use of other information in the image.

In this paper, a weighted total variation sparse transform is proposed. The weight of the operators are measured by facilitating the gray scale difference and space distance between the pixels in the image, so as to make the reconstructed CT images obtain more accurate sparse expression.

5.2 Modified weighted total variation

Conventional TV uses local information and assigns a weighted penalty at a constant rate. The modified weighted TV modified (Liu et al. 2012[26]) considers the gray values of adjacent pixels and carries out comparison with associated pixels in succession. Pixels that differ less are assigned a greater weight (larger differences receive smaller weight). σ are standard deviations based on gaussian function, representing image brightness weight coefficient parameter respectively, In this experiment we define that σ =0.09 so that it can lead to the best effect of image.

The specific WTV expression is as follows:

$$\|f\|_{WTV} = \sum_{m,n} \sqrt{W_{m-1,,n}(f_{m,n}-f_{m-1,n})^2 + W_{m,,n-1}(f_{m,n}-f_{m.n-1})^2}$$

Where, $\boldsymbol{w_{m-1,n}} = \mathbf{exp}\left[-\left(\frac{N(\mathbf{f})_{m,n}-N(\mathbf{f})_{m-1,n}}{\sigma}\right)^2\right]$

and $\boldsymbol{w_{m,,n-1}} = \mathbf{exp}\left[-\left(\frac{N(\mathbf{f})_{m,n}-N(\mathbf{f})_{m,n-1}}{\sigma}\right)^2\right]$

The calculation formula for the first order derivative of WTV is:

$$\frac{\partial\|\mathrm{f}\|_{\mathrm{WTV}}}{\partial \mathrm{f}_{\mathrm{m,n}}} \approx \frac{2\mathrm{w}_{\mathrm{m-1,n}}\left(\mathrm{f}_{\mathrm{m,n}}-\mathrm{f}_{\mathrm{m-1,n}}\right)+2\mathrm{w}_{\mathrm{m,n-1}}\left(\mathrm{f}_{\mathrm{m,n}}-\mathrm{f}_{\mathrm{m,n-1}}\right)}{\sqrt{\varepsilon+\mathrm{w}_{\mathrm{m-1,n}}\left(\mathrm{f}_{\mathrm{m,n}}-\mathrm{f}_{\mathrm{m-1,n}}\right)^2+\mathrm{w}_{\mathrm{m,n-1}}\left(\mathrm{f}_{\mathrm{m,n}}-\mathrm{f}_{\mathrm{m,n-1}}\right)^2}}$$

$$-\frac{2w_{m+1,n}\left(f_{m+1,n}-f_{m,n}\right)}{\sqrt{\varepsilon+w_{m+1,n}\left(f_{m+1,n}-f_{m,n}\right)^2+w_{m+1,n}\left(f_{m+1,n}-f_{m+1,n}\right)^2}}$$

$$-\frac{2w_{m,n+1}\left(f_{m,n+1}-f_{m,n}\right)}{\sqrt{\varepsilon+w_{m,n+1}\left(f_{m,n+1}-f_{m,n}\right)^2+w_{m-1,n+1}\left(f_{m-1,n+1}-f_{m,n}\right)^2}}$$

5.3 ART-WTV algorithm

High-quality images similar to the structure of the reconstructed image were used as a prior image. Prior experience was used to limit the range of reconstructed pixel values to [0, 1]. Calculating the TV minimization aimed for employing the improved weighted total variation in the above text.

The mathematical expression of the proposed technique is as follows:

$$\hat{f} = \text{argmin}\ (\|f\|_{\text{WTV}}+\beta*\text{U}(f_{m,n},f_{p\text{-}median})_{\text{PI}})$$

Where, $U\left(f_{m,n},f_{p-median}\right)_{\text{PI}} = \exp\left[-\left(\frac{\left|f_{m,n}-f_{p-median}\right|}{\sigma_r}\right)^2\right]$

where $f_{\text{median}}^{\text{p}}$ represents the value of the element closest to the prior image pixel and the element to be reconstructed $f_{m,n}$. We use a neighbor pixel of pixels to be reconstructed to sort according to pixel values, and then use either the median or mean. β, and σ_d represent the weight factor, and in this experiment we define that $\sigma_r = 0.15$, and $\beta = 0.25$, which can lead to the best effect on image. For convergence with a successive approximation, after finding TV, the convergence reconstruction is obtained using a linear combination to obtain f_{ART}^{k+1} from pixel values of this f_{ART}^{k} and the last f_{ART}^{k-1}which will be used as an initial value for iteratively updating the next cycle, where the initial value of t^k is 1.

The algorithm is summarized below:

Step 1: Read in the image and initialize the image to be estimated.

Step 2: Reconstruct the image with an ART algorithm.

$$f_{ART}^{k+1} = f_{ART}^{k} + w(i)\frac{P(i)-w(i)f_{ART}^{k}}{w(i)*w(i)}$$

Step 3: Based on the prior image, set the range of pixel values [min, max] for the image, and carry out correction to the variable in Step 2.

$$f_{ART}^{k} = \begin{cases} min, & f_{ART}^{k} < min \\ max, & f_{ART}^{k} \geq max \end{cases}$$

Step 4: If the Euclidean distance between the pixel of the image processed with of the ART

reconstruction method and the pixel before processing the image meet

$\frac{\|f^{k+1}-f^{k}\|}{\|f^{k}\|} > \varepsilon$ (ε is a smaller positive number set artifically, take ε=10^{-8}),

proceed to Step 5. Otherwise go to end.

Step 5: Solve weight function $w_{,m-1,n,n}$

Step 6: $f^{K}_{p-median}$= median $\{f^{k}_{m,n}; (m,n) \in \Omega\}$

Step 7: Function $U(f_{m,n}, f_{p-median})$derivation $: \frac{\partial\ U(f_{m,n},f_{p-median})_{PI}}{\partial f_{m,n},}$

Step 8: Solve the minimization of WTV function.

$$f_{WTV}^{k,l} = f_{WTV}^{k,l-1} - \lambda * da * \frac{\upsilon_{WTV}^{k,l-1}}{\|\upsilon_{WTV}^{k,l-1}\|}$$

$$f_{WTV}^{k} = f_{WTV}^{k} + \beta * U(f_{m,n}, f_{p-median})_{PI}'$$

$$f_{ART}^{k+1} \leftarrow f_{WTV}^{k}$$

Step 9: Linear combination acceleration.

$$f_{ART}^{k+2} = f_{ART}^{k+1} + \frac{t^{k}-1}{t^{k}}(f_{ART}^{k+1} - f_{ART}^{k})$$

$$t^{k+1} = \frac{1+\sqrt{1+4*(t^{k})^{2}}}{2}$$

$$t^{k} \leftarrow t^{k+1}$$

5.4 Comparison of Algorithm Based on Incomplete Projection Reconstruction

5.4.1. Reconstruction Algorithm of CT with Sparse Projection

The projection data collection was restricted at 90°, 60° and 45° view directions at the sampling range of 0° -180° and reconstructed image quality was compared between FBP, ART-TV, EM-TV and our proposed technique. The iterations were set at 100, 200, 300, 500 and 1,000. Differences in reconstructed images were not so large for iteration times of larger than 100, so that iteration times for all processing algorithms were set at 100. For ART-TV and EM-TV algorithms, λ value was set at 0.5.

Fig. 12 shows reconstructed images by various reconstruction algorithms and their settings. Fig. 4 shows that streak-like artifacts significantly appeared reconstructed on images reconstructed by the FBP algorithm and such artifacts were slightly appeared on images processed by ART-TV and EM-TV algorithms at reduced view directions (60° and 45°) at the sampling range of 0° -180°. However, our proposed methods suppressed such streak-like artifacts.

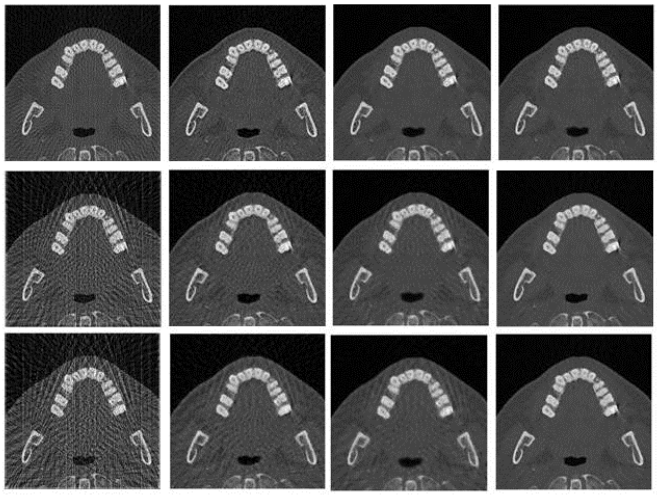

Fig. 12: Reconstructed images from the original image, which is shown in Fig. 4, left. The projection data were collected in the range of 0° to 180°. The number of projection data were 90 (top row), 60 (middle row), 45 (bottom row) since sampling intervals were set at 2°, 3°, 4° by equal thinning. Reconstruction algorithms were, FBP, ART-TV, EM-TV, and our proposed method, from far left column to far right column, respectively.

Fig. 12 shows an image noise index, normalized mean square error (NMSE). Results showed lower values at EM-TV and lower values at reduced view directions, 45°.

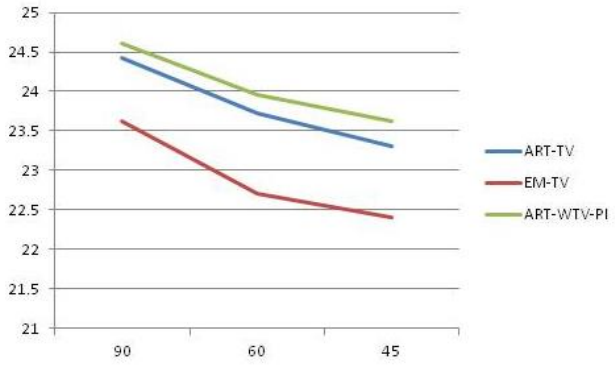

Fig. 13: Image noise index, NMSE, corresponding to different reconstruction methods and settings in Fig. 2. Three values, 90, 60 and 45 on the axis of abscissas are the number of projection data. ART-WTV-PI is our proposed method.

5.4.2 Reconstruction Algorithm of CT with Incomplete Projection

Figs. 14 and 15 shows reconstructed images by various reconstruction algorithms and their settings, especially varying the angle range (less than 180°) of the projection data collection.

Figs. 14 and 15 reconstruction images with 90 view projection direction.

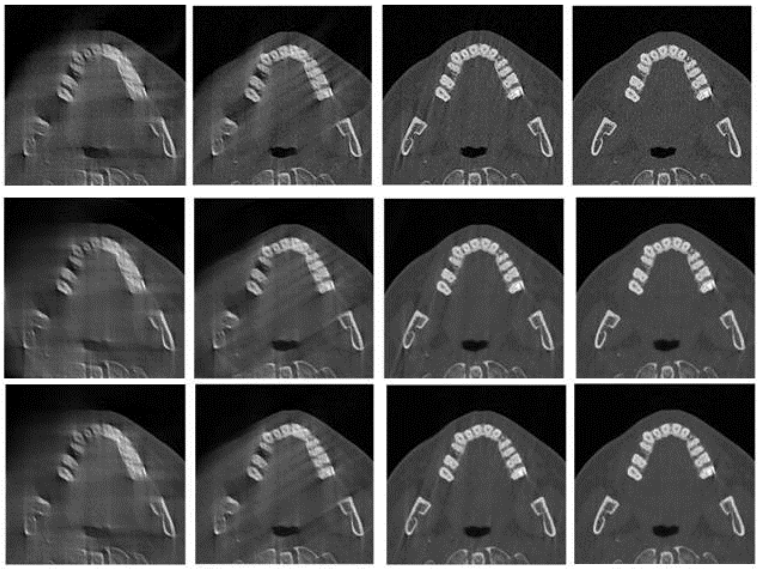

Fig. 14: Reconstructed images from the original image, which is shown in Fig. 4, left. The projection data were collected in the angle range of 0° to 110°, 0° to 130°, 0° to 150°, 0° to 170°, from far left column to far right column, respectively. Reconstruction algorithms were, ART-TV (top row), EM-TV (middle row), and our proposed method (bottom row).

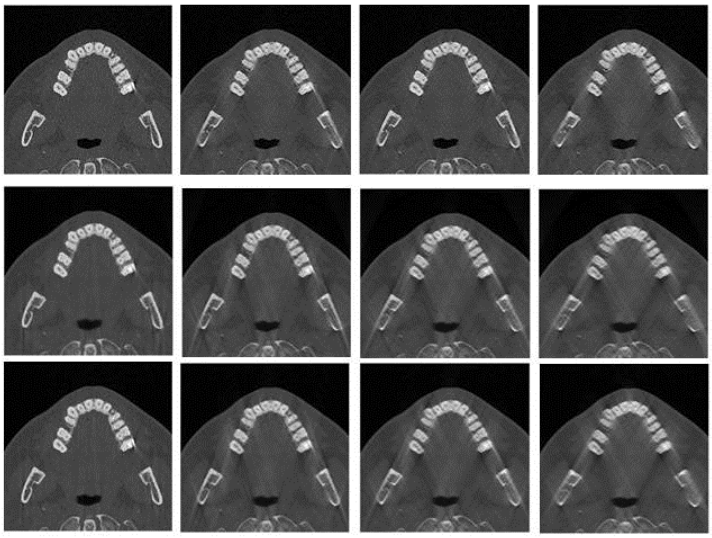

Fig. 15: Reconstructed images from the original image, which is shown in Fig. 4, left. The projection data were collected in the angle range of 5°-175°, 15°-165°, 25°-160°, 35°-155°, from far left column to far right column, respectively. Reconstruction algorithms were, ART-TV (top row), EM-TV (middle row), and our proposed method (bottom row).

As shown in Fig. 14, when the angle range of the projection data collection were changed from 0° to 110°, 0° to 130°, 0° to 150° to 0° to 170°, all reconstructed images keep the quality

at the range, 0° to 170°, only. In addition, both the EM-TV and our proposed methods also provided the high quality at 0° to 150°. These images have comparative image quality with the original image, which is shown in Fig.6, left. On other images, severe blurring and slight distortion on the right maxilla and right mandibular ramus regions were observed.

As shown in Fig. 15, when the angle range of the projection data collection were changed from 5° to 175°, 15° to 165°, 25° to 160° to 35° to 155°, reconstructed images became blurring except for those at 5° to 175° (far left column) for all three reconstruction algorithms. However, on other images severe blurring and slight distortion were observed.

5.5 Discussion

This is a study to explore the optimized X-ray CT reconstruction algorithms for the sparse projection data at various settings. Our proposed method was a modified algorithm for the X-ray CT image reconstruction to improve the quality of restored images. Our proposed method was essentially made of the combination with a weighted TV (WTV) algorithm (Liu et al. 2012[26]) and PICCS (Chen et al. 2008; Nett et al. 2008[16-17]) as described in the Method section.

Algebraic Reconstruction Technique based on the TV regularization pattern has confirmed the effectiveness on the X-ray CT reconstruction using sparse projection angles. However, the traditional TV pattern doesn't take the differences between pixels into consideration, applying the same and even weighing on pixels, and making the edge of pictures too smooth. By contrast, the method put forward in this paper, through the complete search of neighboring pixels, increases the uneven weighing on the similarity of neighboring pixels and integrates the limitation of prior image. Thus, it is restraining the strip artifact more effectively while keeping the details of pictures, achieving reconstructed image with higher precision.

The examination was carried out using a clinical dento-alveolar CT slice (MDCT slice in maxilla). As shown in Fig. 14, the sparse projection data collection, such as 60 and 45 view directions at the sampling range of 0° -180°, streak-like artifacts are not avoidable with the FPB algorithm. Artifacts were significantly suppressed by ART-TV, EM-TV and our methods. However, weak streak-like artifacts are also observed on reconstructed images by the ART-TV and EM-TV algorithms. But, such artifacts are not shown on the image processed by our proposal method, which is shown at the bottom of the far right column in Fig. 4.

Image noise index, NMSE, was shown in Fig. 15. Our proposed method does not always show the good performance in comparison with the EM-TV algorithm, but it was compatible with the ART-TV algorithm. However, on the other hand, the occurrence of the streak-like

artifacts was dramatically changed between reconstruction algorithms. We thought that the recognition of fine anatomical structures was not seriously affected by the noise level difference in artifact-free images in the study.

Figs. 14 and 15 show quality changes in reconstructed images by various reconstruction algorithms and their settings, especially varying the angle range (less than 180°) of the projection data collection. As shown in Fig. 4, by increasing the angle range of the projection data collection were changed from 0° to 110° to 0° to 170°, all reconstructed images showed better quality. Especially both the EM-TV and our proposed methods provided the high quality at 0° to 150° in addition to 0° - 170°. These images have comparative image quality with the original image (Fig. 4, left). As shown in Fig. 5, the production of high-quality images was archived at 5° to 175° for three reconstruction algorithms. The blurring images in Fig. 4 and 5 indicates that the optimization in our proposal method is necessary. However, the trial to use the reduced angle range of the projection data collection, less than 180°, seems to be novel, and got good image quality at 170° (0° - 170° and 0° - 170°) and at 0° to 150° .

Results of the EM-TV algorithm showed a good performance as similar as that of our proposed method in Figs. 14 and 15. The change the limitation of data consistency in the TV-pocs algorithm to the expectation maximization and putting forward the expectation maximization-total variation (EM-TV) algorithm was indicated as an application to PET imaging (Sawatzky et al. 2008; Yan et al. 2011[27-28]).

The total variation regularization based on the compressed sensing theory makes possible keep the X-ray CT image quality high even if the low dose exposure to patients were carried out. We studied the possibility of the combination of a prior image constrained compressed sensing (PICCS) reconstruction method (Chen et al. 2008; Nett et al. 2008[16-17]) and a weighted TV (WTV) algorithm (Liu et al. 2012[26]) and the application on a clinical CT image on maxilla. Our proposed method apparently outperformed the ART-TV algorithm in streak-like artifact reduction and signal-to-noise ratio. Compared with the TV conversion, the amount of calculation increased due to the following reasons: (1) Search range in the calculation of weighting function is increased. (2) In order to achieve the balance between image quality and calculation amount, the search range can be limited to 7×7 pixels around each pixel. (3) Calculation of limiting prior image is added. (4) Although the linear accelerated calculation is added, the effect is not very obvious.

5.6 Conclusion

X-ray CT reconstruction using various sparse projection data was examined with ART-TV,

EM-TV, and our proposed method, which is the combination of a prior image constrained compressed sensing reconstruction method and a weighted TV algorithm. Our proposed method was always outperformed the ART-TV and EM-TV algorithms in streak-like artifact reduction and compatible in signal-to-noise ratio characteristics. With restrained projection, similar quality images with the original image were reconstructed using projection data in a sampling range of 0° to 170° and 5° to 175°. However, ART-TV and EM-TV algorithms caused serious blurring. Therefore, our strategy seems to be a solution to provide high-quality X-ray CT image reconstructed from incomplete projection data.

Chapter 6. Research summary

With the development of CT technology, traditional CT reconstruction algorithms such as FBP，ART and ML_EM can not reconstruct images to be used in clinical diagnosis on the condition of sparse projection . Compressed sensing principle has solved this problem and thus becomes the research focus in the field of CT Imaging. If the image is sparse or can be sparsely showed, the original image can be accurately recovered through appropriate optimization with data less than full sampling.

Since the compressed sensing theory was raised in 2006, CT algorithms based on Compressed Sensing have made great progress. And CT reconstruction algorithm based on Total Variation has received attention due to its simple operation and good effect. However, there are some deficiencies in this algorithm. We performed some researches to solve these problems. After comparing the reconstruction effects of CT reconstruction algorithm with incomplete projection, we found the existing reconstruction method based on Prior Image Constrained Sensing(PICCS) may provide an improved reconstruction quality based on experimental results.

The main research results of this paper include:

1. The comparison of reconstruction results between traditional CT reconstruction algorithm, and the study of ART_TV algorithm in the condition of sparse projection. Experiment results show that reconstruction done by algebraic iterative method got best results, among all the traditional reconstruction algorithms in the condition of sparse projection. But the improvement was limited due to the long running period. Compared to traditional CT reconstruction algorithms, ART_TV's reconstructed images have higher imaging quality with excellent contrast even if it is under 36 projection data.

2. Methods of Prior Image Constrained Sensing, PICCS, reconstruction are studied. We

found that sparse transformation conducted on image of Total Variation, TV, transformation would make edge of the image too smooth. We may make full use of the center point of the region, and the brightness difference and distance of adjacent pixels to calculate the weight of TV more accurately. Thus, we proposed an improved CT image reconstruction algorithm combining WTV and PICCS to guarantee that the reconstructing CT image would become more sparse. Experiment results show that CT image of a higher quality can be reconstructed in the condition of sparse projection. This is more suitable for the reconstruction of sparse projection data, and images of high quality can still be reconstructed in the condition of limiting the reconstruction of projection data with a projection range of 5 to 175 degrees,

Generally, our research demonstrates that CT reconstruction algorithm based on Compressed Sensing has important academic and practical values in reducing X-ray radiation on patients during CT scan, and improving the quality of CT images.

References

1. Radon J:On the determination of functions from their integral values along certain manifolds.IEEE Trans Med Imag 5:170-176,1986.
2. Kondo A, Hayakawa Y, Dong J, Honda A. Iterative correction applied to streak artifact reduction in an X-ray computed tomography image of the dento-alveolar region. Oral Radiol. 2010;26:61-5.
3. Dong J, Kondo A, Abe K, Hayakawa Y: Successive iterative restoration applied to streak artifact reduction in X-ray CT image of dento-alveolar region. Intl J of Comp Assist Radiol Surg. 2011;6:635-40.
4. Dong J, Hayakawa Y, Kannenberg S, Kober C. Metal-induced streak artifact reduction using iterative reconstruction algorithms in X-ray CT image of the dento-alveolar region. Oral Surg Oral Med Oral Pathol Oral Radiol. 2013;115:e63-73.
5. Dong J, Hayakawa Y, Kober C. Statistical iterative reconstruction for streak artefact reduction when using multi-detector CT to image the dento-alveolar structures. Dentomaxillofacial Radiol. 2014;43:20130373.
6. Gordon R， Bender R， Herman G . Algebraic reconstruction techniques (ART) for three-dimensional electron microscopy and X-ray photography. J Theor boil, 1970,29(3):471-476
7. A. H Andersen. Algebraic reconstruction in CT from limited views, IEEE Trans, 1989, 8(2): 50-55.

8. Herman G.T., Meyer L.B. Algebraic reconstruction techniques can be made computationally efficient. IEEE Transactions on Medical Imaging. 1993, 12(3): 600-609.
9. Candes EJ, Romberg J, Tao T. Robust uncertainty principles: exact signal reconstruction from highly incomplete frequency information. IEEE Trans Inform, Theory 2006, 52(2): 489-509.
10. Donoho, DL. Compressed sensing. IEEE Transactions on Information Theory. 2006; 52:1289-306.
11. Rudin L I, Osher S, Fatemi E. Nonlinear total variation based noise removal algorithms. Physica D: Nonlinear Phenomena, 1992, 60(1-4): 259-268.
12. Baraniuk, RG, Candes E, Elad M, Ma Y. (Eds.). Special Issue on: Applications of Sparse Representation and Compressive Sensing. Proceedings of the IEEE. 2010;98:906-1101.
13. Kudo H, Suzuki T, Rashed EA. Image reconstruction for sparse-view CT and interior CT – introduction to compressed sensing and differentiated backprojection. Quant Imag Med Surg, 2013;3:147-61. doi: 10.3978/j.issn.2223-4292.2013.06.01
14. Sidky EY, Pan X. Image reconstruction in circular cone-beam computed tomography by constrained, total-variation minimization. Phys Med Biol. 2008:53:4777-807. doi: 10.1088/0031-9155/53/17/021
15. Sidky EY, Kao ,CM Pan X. Accurate image reconstruction from few-views and limited-angle data in divergent-beam CT. Jouranl of X-Ray Science and Technology, 2006,14(2):119-139.
16. Chen Guang-Hong,Jie T,Shuai L.Prior image constrained compressed sensing (PICCS): A method to accurately reconstruct dynamic CT images from highly under sampled projection datasets. Med Phys,2008,6856(2):685618.
17. Nett B,Tang J,Leng S,et al. Tomosynthesis via total variation minimization reconstruction and prior image constrained compressed sensing (PICCS) on a C-arm system. Singapore: Med Imag,2008:69132D-69142D.
18. Siltanen S, Kolehmainen V, Järvenpää S, Kaipio JP, Koistinen P, Lassas M, et al. Statistical inversion for medical x-ray tomography with few radiographs: I. General theory. Phys Med Biol 2003;48:1437-63.
19. Kolehmainen V, Siltanen S, Järvenpää S, Kaipio JP, Koistinen P, Lassas M, et al. Statistical inversion for medical x-ray tomography with few radiographs: II. Application to dental radiology. Phys Med Biol 2003;48:1465-90.

20. Sidky EY, Kao C-M, Pan X. Accurate image reconstruction from few-views and limited-angle data in divergent-beam CT. J X-Ray Sci Tech, vol. 14, no. 2, pp. 119-139, 2006 (free download at http://arxiv.org/abs/0904.4495v1)
21. Siltanen S, Kolehmainen V, Järvenpää S, Kaipio JP, Koistinen P, Lassas M, et al. Statistical inversion for medical x-ray tomography with few radiographs: I. General theory. Phys Med Biol 2003;48:1437-63.
22. Rose S, Andersen MS, Sidky EY, Pan X. Noise properties of CT images reconstructed by use of constrained total-variation, data-discrepancy minimization. Med Phys. 2015; 42: 2690-8. doi: 10.1118/1.4914148.
23. Dong J, Kudo H: Proposal of compressed sensing using nonlinear sparsifying transform for CT image reconstruction. Med Imag Tech. 2016;34:235-44. http://doi.org/10.11409/mit.34.235
24. Dong J, Kudo H: Accelerated algorithm for compressed sensing using nonlinear sparsifying transform in CT image reconstruction. Med Imag Tech. 2017;35:63-73. http://doi.org/10.11409/mit.35.63
25. Yu W, Wang C, Huang M. Edge-preserving reconstruction from sparse projections of limited-angle computed tomography using ℓ0-regularized gradient prior. Rev Sci Instrum. 2017;88:043703. doi: 10.1063/1.4981132.
26. Liu Y, Ma J, Fan Y, et al. Low-dose computed tomography image reconstruction from under-sampling data based on weighted total variation minimization[J]. Proceedings of SPIE, 2012.
27. Sawatzky A, Brune C, Wubbeling F, Kosters T, Schafers K, Burger M. 2008. Accurate EM-TV algorithm in PET with low SNR. Nuclear Sci. Symp. Conf. Rec. NSS08. IEEE.

Declaration

1. All the images (clinical images) were processed under the patients' consents that they approved the use for image processing in this study.
2. All the institutional review board (IRB) of hospitals (medical institutions) where the processed images were acquired, have approved the clinical image providing.

Acknowledgments

Successful completion of my paper is attributable to teachers' careful guidance. Here, I'd like to express thanks for their efforts. Firstly, I'd like to thank Teacher Zaochuan who led me into the world of graphic processing, and guided me in the reading of professional books and conducting of scientific research. Secondly, I'd like to thank all teachers of Kitami Institute of Technology, who created a good learning atmosphere for us, and offered convenient conditions. And finally, I'd like to thank my family members for their support and encouragement.